Molecular Cell
Article

Rejuvenation of CcdB-Poisoned Gyrase by an Intrinsically Disordered Protein Domain

Natalie De Jonge,[1,3] Abel Garcia-Pino,[1,3] Lieven Buts,[1,3] Sarah Haesaerts,[1,3] Daniel Charlier,[2] Klaus Zangger,[4] Lode Wyns,[1,3] Henri De Greve,[1,3] and Remy Loris[1,3,*]
[1]Structural Biology Brussels
[2]Erfelijkheidsleer en Microbiologie
Vrije Universiteit Brussel, Pleinlaan 2, 1050 Brussels, Belgium
[3]Structural Biology Brussels, Department of Molecular and Cellular Interactions, VIB, Pleinlaan 2, 1050 Brussels, Belgium
[4]Institute of Chemistry, University of Graz, Heinrichstrasse 28, 8010 Graz, Austria
*Correspondence: remy.loris@vib-vub.be
DOI 10.1016/j.molcel.2009.05.025

SUMMARY

Toxin-antitoxin modules are small regulatory circuits that ensure survival of bacterial populations under challenging environmental conditions. The *ccd* toxin-antitoxin module on the F plasmid codes for the toxin CcdB and its antitoxin CcdA. CcdB poisons gyrase while CcdA actively dissociates CcdB:gyrase complexes in a process called rejuvenation. The CcdA:CcdB ratio modulates autorepression of the *ccd* operon. The mechanisms behind both rejuvenation and regulation of expression are poorly understood. We show that CcdA binds consecutively to two partially overlapping sites on CcdB, which differ in affinity by six orders of magnitude. The first, picomolar affinity interaction triggers a conformational change in CcdB that initiates the dissociation of CcdB:gyrase complexes by an allosteric segmental binding mechanism. The second, micromolar affinity binding event regulates expression of the *ccd* operon. Both functions of CcdA, rejuvenation and autoregulation, are mechanistically intertwined and depend crucially on the intrinsically disordered nature of the CcdA C-terminal domain.

INTRODUCTION

The *ccd* operon on the F plasmid of *Escherichia coli* (Miki et al., 1984) is an archetype of the toxin-antitoxin (TA) modules that are present on the chromosomes and plasmids of many bacteria and archaea (Buts et al., 2005b; Pandey and Gerdes, 2005). When present on low-copy-number plasmids, they serve to stabilize the plasmid by a mechanism known as postsegregational killing. In contrast, the biological functions of TA modules residing in bacterial and archaeal chromosomes are the subject of a passionate debate (Magnuson, 2007). One hypothesis states that TA modules act as stress-response elements, ensuring survival of a fraction of the population during episodes of environmental and nutritional stress (Gerdes, 2000; Buts et al., 2005b; Gerdes et al., 2005). Another theory suggests that they are responsible for programmed cell death (Engelberg-Kulka and Glaser, 1999; Kolodkin-Gal et al., 2007; Nariya and Inouye, 2008). Independent of their exact biological role, their potential as targets for the development of novel antibiotics is widely recognized (Engelberg-Kulka et al., 2004; Alonso et al., 2007; Williams and Hergenrother, 2008).

The *ccd* operon on plasmid F encodes two proteins: the toxin CcdB and its antitoxin CcdA. CcdA neutralizes CcdB by forming a noncovalent complex (Maki et al., 1996). This complex further acts as a repressor of the *ccd* operon (Tam and Kline, 1989b). CcdA is a substrate for the Lon protease and is a dimeric, two-domain protein. Its N-terminal dimerization/DNA-binding domain is well structured and adopts a ribbon-helix-helix fold (Madl et al., 2006). On the other hand, its C-terminal domain, which interacts with CcdB, is intrinsically disordered (Bernard and Couturier, 1991; Madl et al., 2006).

The target of CcdB is DNA gyrase, an essential bacterial topoisomerase that can introduce negative supercoils in DNA at the expense of ATP. This enzyme allows the relaxation of positive supercoils ahead of the replication fork and thus ensures the continuation of the replication. Gyrase is a heterotetramer consisting of two GyrA subunits and two GyrB subunits. While GyrA contains the intrinsic DNA supercoiling/relaxing activity, GyrB harbors the associated ATP hydrolysis activity that is required for some, but not all, gyrase-mediated reactions. The 59 kDa N-terminal part of GyrA (GyrA59) contains the active site tyrosines responsible for the DNA breakage and religation. During each cycle of strand passage, the $GyrA59_2$ dimer goes through a number of distinct conformations (Morais Cabral et al., 1997; Dong and Berger, 2007; Fass et al., 1999), one of which (the ''open'' conformation) is recognized by the $CcdB_2$ dimer (Dao-Thi et al., 2005). Binding of $CcdB_2$ to $GyrA59_2$ prevents strand passage as well as closure of the enzyme (Critchlow et al., 1997). CcdB can both inhibit free gyrase and stabilize covalent gyrase:DNA intermediates (Bernard and Couturier, 1992), creating a roadblock for polymerases. CcdB-poisoned gyrase complexes can be resolved by CcdA in a poorly understood process termed rejuvenation (Maki et al., 1996; Bernard et al., 1993). It remains unclear how rejuvenation can be accomplished through a simple competition between CcdA and gyrase for the same binding site on CcdB.

The affinity of CcdA for its operator DNA is modulated by the ratio between CcdA and CcdB. Both $CcdA_2$ and $CcdB_2$ are thought to posses two binding sites for each other, allowing

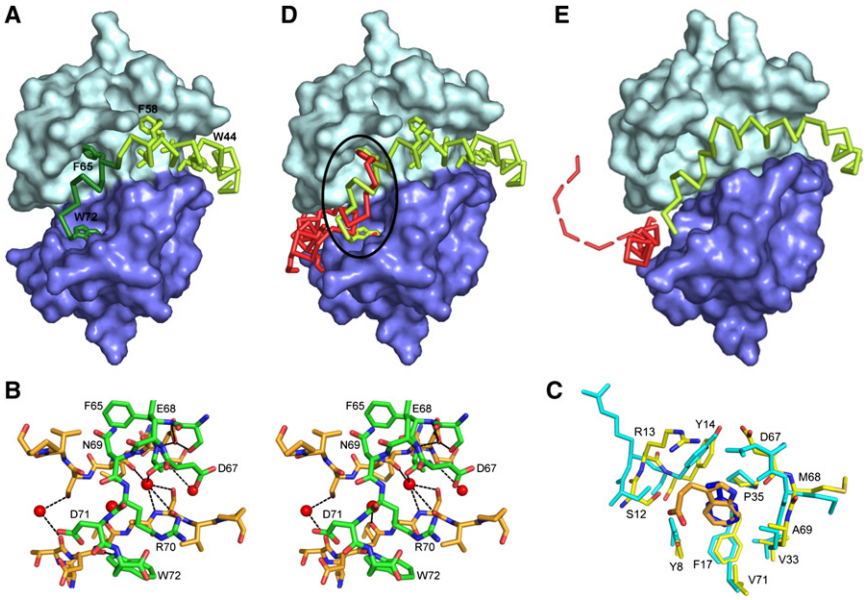

Figure 1. Crystal Structures of the $CcdB_2$:$CcdA^{37-72}$ and $CcdB_2$:$CcdA^{37-72}{}_2$ Complexes

(A) Architecture of the $CcdB_2$:$CcdA^{37-72}$ complex. The $CcdB_2$ dimer is shown as a surface representation with the two monomers in different shades of blue. $CcdA^{37-72}$ is shown as a Cα trace, with segment Ser64-Trp72 colored dark green and segment Arg40-Gly63 in light green. The side chains of all hydrophobic residues of $CcdA^{37-72}$ are shown in stick representation and the aromatic residues (Trp44, Phe58, Phe65, and Trp72) are labeled.

(B) Detailed stereoview of the interaction of the $CcdA^{65-72}$ segment (green) with the $CcdB_2$ dimer interface (orange). CcdA residues are labeled. The peptide makes a number of direct and water-mediated hydrogen bonds with $CcdB_2$ (dashed lines).

(C) The aromatic binding pocket of CcdB can accommodate both Phe65 and Trp72 of $CcdA^{37-72}$. The symmetrically disposed aromatic binding pockets of $CcdB_2$ are superposed and shown in stick representation. Residues corresponding to monomer A of $CcdB_2$ are shown in cyan and interact with the side chain of Phe65 (blue). Residues corresponding to the aromatic binding pocket of monomer B of $CcdB_2$ are shown in yellow and interact with the side chain of Trp72 of $CcdA^{37-72}$ (orange).

(D) Symmetric positioning of a second $CcdA^{37-72}$ on the $CcdB_2$ dimer. Positioning of a second $CcdA^{37-72}$ monomer (red) on the symmetry-related binding site results in sterical hindrance for the Ser64-Trp72 segment.

(E) Crystal structure of the $CcdB_2$:$CcdA^{37-72}{}_2$ complex. This structure shows that two Arg40-Met61 segments, but only a single Ser64-Trp72 segment, bind in the CcdA-binding groove. The Ser62-Trp72 segment of the other $CcdA^{37-72}$ domain remains unbound and intrinsically disordered (represented by a dashed line).

the formation of complexes with different stoichiometries (Dao-Thi et al., 2002). Maximal repression is achieved at CcdB:CcdA ratios of one (Afif et al., 2001). The repressing complex is supposed to consist of a chain of alternating $CcdA_2$ and $CcdB_2$ dimers (Dao-Thi et al., 2002). At higher ratios, CcdB acts as an antirepressor rather than a corepressor, resulting in a soluble hexameric $CcdA_2$:$CcdB_4$ complex. This phenomenon is general for all TA modules and has been termed conditional cooperativity (Overgaard et al., 2008; Johnson et al., 1996; Magnuson and Yarmolinsky, 1998; Afif et al., 2001; Monti et al., 2007). The structural and energetic basis behind conditional cooperativity remains unknown.

Although the structures of the $CcdA_2$ and $CcdB_2$ dimers in their unbound states (Madl et al., 2006; Maki et al., 1996; Loris et al., 1999) and of the $CcdB_2$ dimer in complex with a relevant fragment of gyrase (GyrA14) (Dao-Thi et al., 2005) are known, a structure of a CcdB:CcdA complex was missing. Furthermore, different affinity constants have been published for the interactions between CcdA and CcdB (Dao-Thi et al., 2002, 2005; Kampranis et al., 1999). Titrations in different directions result in different apparent stoichiometries and affinities, indicating that equilibrium is not reached during the experiment (Dao-Thi et al., 2002). The presumed origin of this kinetic barrier is the bivalency of both the $CcdA_2$ and $CcdB_2$ dimer for each other. We therefore decided to reduce the complexity of the system by working with the monomeric C-terminal domain of CcdA only, which we call $CcdA^{37-72}$, as it consists of residues Arg37 to Trp72 of CcdA. Here, we present structural and biophysical data on the interaction between CcdB and $CcdA^{37-72}$ that unveil the mechanism behind the rejuvenation process and mechanistically link it to the regulation of expression of the *ccd* operon.

RESULTS

Architecture of the $CcdB_2$:$CcdA^{37-72}$ and the $CcdB_2$:$CcdA^{37-72}{}_2$ Complexes

In solution, $CcdA^{37-72}$ behaves as a monomeric and intrinsically disordered protein and folds upon binding to CcdB (Supplemental Experimental Procedures and Figures S1 and S2 available online). The crystal structure of the $CcdB_2$:$CcdA^{37-72}$ complex is asymmetric with a single $CcdA^{37-72}$ domain wrapped around the $CcdB_2$ dimer in a largely α-helical conformation, burying a total combined molecular surface of 2850 $Å^2$ for $CcdA^{37-72}$ and $CcdB_2$ (Figure 1A). Electron density is observed for residues Ala41-Trp72, while residues Arg37-Arg40 remain disordered (Figures S3A and S3B). $CcdA^{37-72}$ in this complex can be divided into two segments. Segment Arg40-Gly63 forms a long bent α-helix. The interaction surface on $CcdB_2$ for this segment is largely hydrophobic and accounts for about half of the buried surface area. Only two intermolecular hydrogen bonds are formed with the $CcdB_2$ dimer. Segment Ser64-Trp72, on the other hand, has a more irregular structure harboring just a single helical turn at its center. The latter nine-residue segment traverses the border between the two CcdB monomers, thus breaking the structural symmetry. It is bound intimately and accounts on its own for about 1400 $Å^2$ of buried surface area. Its interface is of a more mixed hydrophilic/hydrophobic nature and includes a series of 9 direct intermolecular hydrogen bonds and a large number of water bridges. A number

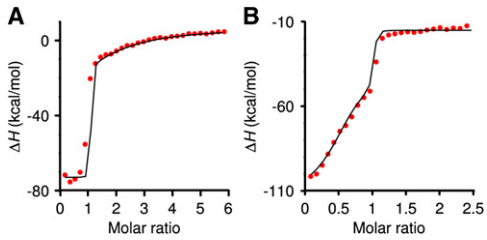

Figure 2. ITC Measurements Show a Biphasic Behavior

(A) The titration of $CcdA^{37-72}$ into $CcdB_2$ shows a first high-affinity binding event (steep slope) followed by a second lower-affinity binding event (shallow slope).

(B) The reverse titration of $CcdB_2$ into $CcdA^{37-72}$ equally shows a clear biphasic profile. Here the first phase corresponds to both the high- and low-affinity binding sites of $CcdB_2$ interacting with excess $CcdA^{37-72}$. The second phase corresponds to a switch of $CcdA^{37-72}$ from the low-affinity binding site toward the high-affinity binding site when excess $CcdB_2$ is titrated into the cell. Although significant cross-correlation limits the accuracy of the derived model parameters, it is clear that the two dissociation constants must differ by at least 6 orders of magnitude.

of these water bridges occur at the dimer interface of $CcdB_2$ (Figure 1B) and relate to the $CcdA^{37-72}$-induced change in quaternary structure of $CcdB_2$ (see below). Remarkably, the two aromatic side chains of the Ser64-Trp72 segment (Phe65 and Trp72) are located in identical hydrophobic pockets on the $CcdB_2$ surface, each belonging to a different CcdB subunit (Figure 1C). Small differences in the side chain conformations of the CcdB residues involved, in particular Tyr8 and Tyr14, optimize binding for the two aromatic side chains Phe65 and Trp72 of $CcdA^{37-72}$ and allow for the accommodation of the free carboxylate group of the C-terminal Trp72.

Modeling of a second $CcdA^{37-72}$ fragment in the same conformation on the $CcdB_2$:$CcdA^{37-72}$ complex results in severe steric overlap between their respective Phe64-Trp72 segments (Figure 1D). How a second $CcdA^{37-72}$ domain can be accommodated by $CcdB_2$ is explained by our second crystal structure. The asymmetric unit of these crystals contains a single $CcdB_2$:$CcdA^{37-72}{}_2$ complex (Table 1). The crystal structure shows that the symmetrically positioned, but partially excluded, second binding site only accommodates residues Arg40-Gly61 of $CcdA^{37-72}$, while residues Ser62-Trp72 remain unbound and disordered (Figure 1E). In the crystal structure, both Ser62-Trp72 segments are visible in the electron density, but only at half occupancy (Figures S3C and S3D). This second binding site on $CcdB_2$ makes it possible to form a linear alternating $(CcdB_2{:}CcdA_2)_n$ chain on the operator DNA. Such a chain has been proposed by several authors as the most likely repressor complex (Madl et al., 2006; Dao-Thi et al., 2002; Afif et al., 2001).

The $CcdB_2$ Dimer Carries a High- and a Low-Affinity Binding Site

Our crystal structures of $CcdB_2$ in complex with $CcdA^{37-72}$ suggest a consecutive binding model with two distinct affinities. Binding studies using ITC, SPR, CD-, and fluorescence spectroscopy consistently yield a picture of the $CcdB_2$ dimer possessing two binding sites for $CcdA^{37-72}$, differing in affinity by a factor of at least 10^6 (Figure 2 and Figure S4). This is in full agreement with our crystallographic data showing two partly overlapping binding sites for $CcdA^{37-72}$. In our consecutive binding model, the high affinity binding site, which recruits the full length of the $CcdA^{37-72}$ domain, corresponds to a dissociation constant of at least 20 pM. The subsequent low affinity binding event corresponds to a K_D of only 13 μM and involves only residues 40–61.

Further support for this model comes from titrations with the two individual segments of the CcdA C-terminal domain: $CcdA^{37-62}$ and $CcdA^{65-72}$. SPR and CD spectroscopy binding studies show that two $CcdA^{37-62}$ fragments can bind to a $CcdB_2$ dimer with roughly equal micromolar affinities (Figures S4C and S4D). The binding constant for the second binding event of $CcdA^{37-72}$ to $CcdB_2$ agrees well with the binding constants obtained for the $CcdA^{37-62}$ fragment, as would be expected based on the crystal structures. On the other hand, SPR and fluorescence spectroscopy binding studies show that only a single molecule of the C-terminal fragment $CcdA^{65-72}$ can bind to $CcdB_2$, with micromolar affinity (Figures S4E and S4F).

Rejuvenation Requires Only a Single $CcdA^{37-72}$ Equivalent

To ascertain the biological significance of the crystal structure of the $CcdB_2$:$CcdA^{37-72}$ complex, in vivo neutralization experiments and in vitro rejuvenation experiments were performed with the $CcdA^{37-72}$ fragment. We found that coexpression with $CcdA^{37-72}$ is sufficient to protect *E. coli* cells from CcdB. The growth of cells cotransformed with plasmids coding for CcdB and $CcdA^{37-72}$ (efficiency of plating [EOP] = 0.9 ± 0.2) is similar to the growth of cells transformed with plasmids coding for CcdB and full-length CcdA (EOP = 0.8 ± 0.3). Cells transformed with a plasmid coding only for CcdB produce very few colonies (EOP = 0.002 ± 0.002). $CcdA^{37-72}$ is also capable of extracting CcdB from a preformed $GyrA59_2$:$CcdB_2$ complex in an SPR-based assay, indicating that this isolated domain of CcdA indeed possesses the full rejuvenation activity of the full-length protein (Figures 3A and 3B; for definitions of gyrase fragments, see Figure S5).

In order to determine how many molar equivalents of $CcdA^{37-72}$ are required to disrupt the $GyrA59_2$:$CcdB_2$ complex, we performed a series of analytical gel filtration experiments where $GyrA59_2$:$CcdB_2$ was preincubated with different molar equivalents of $CcdA^{37-72}$. Adding a single equivalent of monomeric $CcdA^{37-72}$ to $GyrA59_2$:$CcdB_2$ fully dissociated this complex, producing $GyrA59_2$ and $CcdB_2$:$CcdA^{37-72}$ (Figure 3C), confirming the functional relevance of our crystal structure. This result directly links the high-affinity interaction between CcdB and $CcdA^{37-72}$ to the rejuvenation process.

Rejuvenation Is an Allosteric Process

Comparing the interaction surfaces of $CcdB_2$ in complex with $CcdA^{37-72}$ or $GyrA59_2$ shows that both binding epitopes on CcdB are partly separated. Only the surface of CcdB that interacts with the N-terminus of the $CcdA^{37-72}$ (residues 40–61) overlaps with the GyrA59 interaction surface (Figures 4A and 4B). The binding surface for the C-terminal segment of CcdA, encompassing residues Met61-Trp72, however, remains accessible in

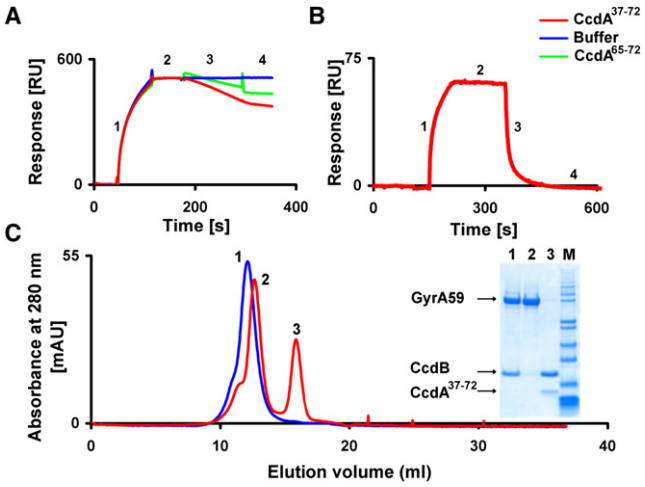

Figure 3. Rejuvenation of the $GyrA59_2$:$CcdB_2$ Complex

(A) SPR experiments show that injections with $CcdA^{37-72}$ and $CcdA^{65-72}$ at concentrations corresponding to 20 times their K_D for $CcdB_2$ result in partial dissociation of the $GyrA59_2$:$CcdB_2$ complex. $GyrA59_2$ was immobilized and saturated with $CcdB_2$ (1). This $CcdB_2$:$GyrA59_2$ complex is stable, and no dissociation is observed (2). Injections with $CcdA^{37-72}$ and $CcdA^{65-72}$ at concentrations corresponding to 20 times their K_D for $CcdB_2$ result in partial dissociation of the $CcdB_2$:$GyrA59_2$ complex (3). Further addition of buffer does not result in further dissociation of the $CcdB_2$:$GyrA59_2$ complex (4).

(B) Higher $CcdA^{37-72}$ concentrations (1 μM) result in full and instantaneous dissociation of the $CcdB_2$:$GyrA59_2$ complex (3). Higher concentrations of $CcdA^{65-72}$ are impossible due to solubility problems.

(C) The $GyrA59_2$:$CcdB_2$ complex was analyzed by analytical gel filtration before and after treatment with $CcdA^{37-72}$. The profile of the $GyrA59_2$:$CcdB_2$ complex is shown in blue (peak 1). After addition of a single molar equivalent of $CcdA^{37-72}$, the complex fully dissociates into peak 2, containing free $GyrA59_2$, and peak 3, containing the $CcdB_2$:$CcdA^{37-72}$ complex. The shoulder on the peak corresponding to free $GyrA59_2$ is observed in all $GyrA59_2$ preparations and is attributed to conformational heterogeneity (open and closed form). The content of the peaks is shown on SDS PAGE, with lane M corresponding to the Mark12 Unstained Standard.

both the $GyrA59_2$:$CcdB_2$ model and the experimentally determined $GyrA14_2$:$CcdB_2$ complex (Dao-Thi et al., 2005).

From these observations a segmental binding model for the rejuvenation process emerges in which the C terminus of CcdA, likely the segment Ser64-Trp72, initially binds with a relatively low affinity to gyrase-bound $CcdB_2$ (Figure 5). After or during the subsequent dissociation of the CcdB:gyrase complex, the Arg40-Gly63 segment of CcdA can zip into the binding groove of $CcdB_2$, resulting in a long-lived, high-affinity $CcdB_2$:$CcdA_2$ complex.

$CcdA^{65-72}$, a CcdA fragment that does not overlap with the gyrase binding region (Figure 4B), partially rejuvenates CcdB-poisoned gyrase complexes in vitro (Figure 3A), substantiating the segmental binding model. This observation implies the involvement of an allosteric component in the rejuvenation by CcdA: interactions at the binding site for the $CcdA^{65-72}$ segment modulate binding on a spatially distinct binding site for gyrase. Further evidence for an allosteric action of the $CcdA^{65-72}$ segment rather than a consecutive binding-release-locking model is provided by the kinetics of the rejuvenation process, which is at least four orders of magnitude faster than the spontaneous dissociation of the CcdB:gyrase complex (see Discussion).

Structural Basis of the Allostery

To understand the structural basis of the allostery, we compared the conformations of $CcdB_2$ in the $CcdB_2$:$CcdA^{37-72}$ and $GyrA14_2$:$CcdB_2$ complexes (Dao-Thi et al., 2005). The most conspicuous difference is a change in quaternary structure involving a relative rotation of 12° of the two CcdB monomers in the $CcdB_2$ dimer (Figure 6A). The dimer interface of $CcdB_2$ in its free state consists of a significant amount of hydrophobic contact surface resulting from the hydrophobic core of the protein that runs through the dimer interface. This is surrounded by a series of hydrogen bonding contacts between both monomers, in particular β sheet type hydrogen bonding between the edge strands of the two monomers resulting in a 10 strand dimer-wide β sheet (Loris et al., 1999). This interface is essentially unchanged in the $GyrA14_2$:$CcdB_2$ complex (Dao-Thi et al., 2005). In the $CcdB_2$:$CcdA^{37-72}$ complex, a significant distortion of $CcdB_2$ dimer interface is observed. The dimer-spanning β sheet is disrupted, and a series of water molecules are inserted (Figure 6B). This situation is not likely to have arisen from crystal packing, as this is the region that most intimately interacts with the segment Phe65-Trp72 of $CcdA^{37-72}$, and this interaction involves, among others, water-bridges using the five water molecules inserted into the β sheet of $CcdB_2$ (Figure 1B).

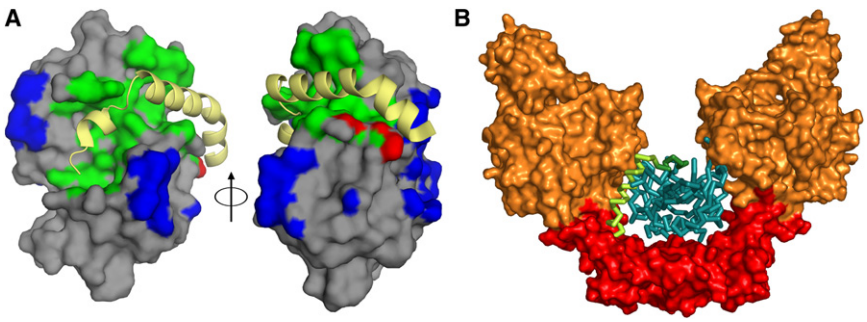

Figure 4. Structural Basis of the Rejuvenation

(A) Surface representation of the $CcdB_2$ dimer with the CcdA interaction surface colored green and the GyrA59 interaction surface colored blue. Overlapping regions between both surfaces are shown in red. The bound $CcdA^{37-72}$ is shown as a yellow ribbon model. Overlap between both interaction surfaces is observed only for the N-terminal segment of $CcdA^{37-72}$.

(B) Composite of the $CcdB_2$:$CcdA^{37-72}$ and $GyrA59_2$:$CcdB_2$ complexes. $GyrA59_2$ is drawn as a surface representation in orange, with its $GyrA14_2$ fragment in red. $CcdB_2$ and $CcdA^{37-72}$ are shown as Cα traces and colored as in Figure 1A ($CcdB_2$ blue and $CcdA^{37-37}$ green). The N-terminus of $CcdA^{37-72}$ points into the $GyrA14_2$ and $GyrA59_2$ fragments, creating a steric conflict for the N-terminal domain of full-length CcdA. A few steric clashes are also formed between segment Arg40-Glu60 of CcdA and GyrA59. No steric constraints are present for segment Met61-Trp72 of CcdA.

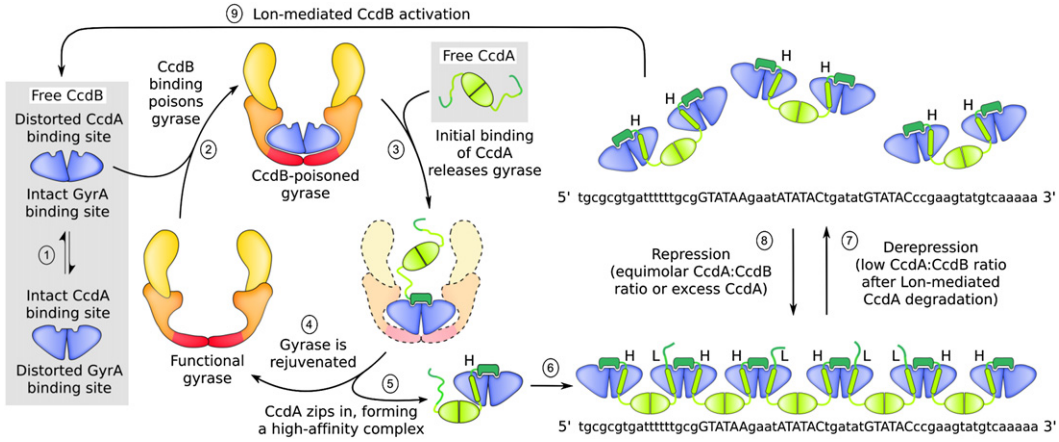

Figure 5. Interaction Diagram for the *ccd* System

Solid shapes represent structured protein domains, while the thinner lines represent domains in an intrinsically disordered state. CcdB (blue) converts between two conformations (1), alternately forming the CcdA- or the GyrA-binding surface. The equilibrium between both CcdB conformations is dictated by the relative affinities of CcdB for GyrA (orange hues) and CcdA (green) and by the concentration of CcdA. When CcdB poisons gyrase (2), a large portion of the $CcdA^{37-72}$-binding surface is shielded and only the $CcdA^{65-72}$ segment can access its binding surface (3). The initial interaction of this segment induces a conformational change in CcdB, releasing it from gyrase (4). After or coincident with CcdB release, the $CcdA^{37-63}$ segment locks onto CcdB (5). The resulting CcdB:CcdA complex is the building block of the repressor complex (6) and forms a chain of alternating $CcdA_2$ and $CcdB_2$ dimers (Dao-Thi et al., 2002). In this complex, both the high-affinity binding site (H) and the partially overlapping low-affinity binding site (L) are occupied. Upon depletion of CcdA by Lon-dependent degradation, excess CcdB resolves the repressor complex to form a soluble hexameric, nonrepressing complex (7), enabling de novo synthesis of CcdA. This results in lower CcdB:CcdA ratios and consequently in rerecruitment of the low-affinity binding site (8), leading to repression of the *ccd* operon. When Lon-mediated CcdA degradation outpaces CcdA synthesis (9), CcdB is eventually freed to poison gyrase.

Furthermore, this conformational change is also present in the crystal structure of the $CcdB_2$:$CcdA^{37-72}{}_2$ complex.

This simple rigid body rearrangement also involves a local conformational change that flips in and out the side chain of Trp99 (Figure S6). The conformational switch involving Trp99 has been described before (Dao-Thi et al., 2005) and serves to create the proper contacts between Trp99 of CcdB and Arg462 of GyrA14 at the core of the binding interface of the $GyrA14_2$:$CcdB_2$ complex. The conformational change further includes loop Thr7-Arg15. This loop is disordered in the $GyrA14_2$:$CcdB_2$ complex (Dao-Thi et al., 2005) but becomes structured in the $CcdB_2$:$CcdA^{37-72}$ complex, forming the hydrophobic pocket that harbors Phe65/Trp72 of $CcdA^{37-72}$. Together, this set of rearrangements cause a switch between a correctly formed CcdA-binding surface and a correctly formed gyrase-binding surface, both of which cannot occur simultaneously (Figure 5). The allosteric component in the rejuvenation process is, thus, essentially of a structural origin.

Autoregulation Depends on the Low-Affinity Binding Site

Although $CcdB_2$ has two binding sites for CcdA, only the high-affinity site is required for the rejuvenation process. We therefore investigated if this second binding site plays a role in the autoregulation. To establish the involvement of the second binding site in the autoregulation, we carried out electrophoretic mobility shift assays (EMSA) with a DNA fragment containing the 113 bp operator/promoter region of the *ccd* operon (O/P) (Tam and Kline, 1989a). Under conditions that promote the formation of an equimolar $(CcdA_2:CcdB_2)_n$ complex, this DNA fragment is shifted (Figure 7), in agreement with previous experiments (Afif et al., 2001). This interaction was challenged by adding increasing amounts of $CcdA^{37-62}$. This fragment, in the concentration range used, is expected to compete for the low-affinity binding site but should not, due to the large difference in affinity, be able to compete for the high-affinity binding site (see Figure S4). This fragment allows us to examine the function of the low-affinity site, while leaving the high-affinity interaction unaffected. Adding competing amounts of $CcdA^{37-62}$ indeed gradually perturbs the shift (Figure 7) under conditions where the high affinity interaction should be retained, indicating the relevance of the low-affinity binding site in the establishment of the repressor complex.

DISCUSSION

CcdA Function Crucially Depends on Intrinsic Disorder

The antitoxins encoded by TA modules typically have a two-domain structure with the C-terminal domain being intrinsically disordered. The latter property is obviously useful to allow easy proteolytic degradation and keeping the in vivo lifetime short, a property essential for fast response to changing environmental conditions. Within the context of the F plasmid *ccd* operon, a short half-life of CcdA is a prerequisite for the postsegregational killing mechanism. Once the plasmid is lost from the bacteria, the antitoxin is quickly degraded while the toxin remains present in the cytoplasm and consequently kills the plasmid-free bacteria.

Segmental and zipper-like binding mechanisms are unique to intrinsically disordered proteins and protein segments (Dunker and Uversky, 2008). In the case of CcdA, rejuvenation requires the consecutive action of two independently acting disordered

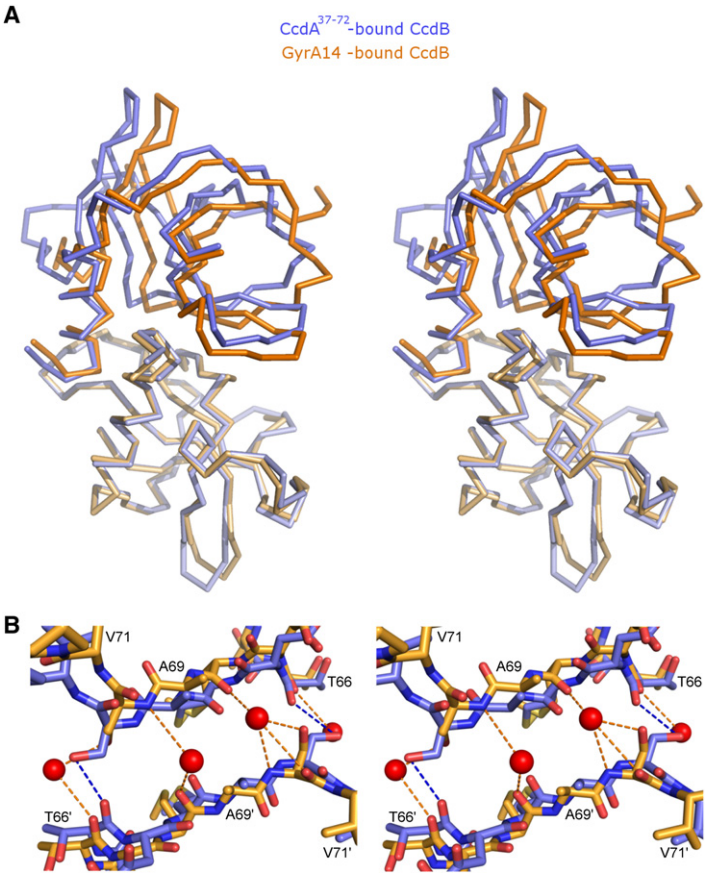

Figure 6. Conformational Changes in the CcdB Dimer

(A) Superposition of $CcdB_2$ in its $GyrA14_2$-bound and $CcdA^{37-72}$-bound conformations. The $CcdB_2$ dimer in its $CcdA^{37-72}$-bound conformation is shown in blue, while the GyrA14-bound conformation is shown in orange. One of the two CcdB monomers was superimposed, and the orientation is chosen to emphasize the rigid body movement of the second CcdB monomer.

(B) Detailed view of the dimer interface for the two extreme conformational states of CcdB. The blue conformation corresponds to gyrase-bound CcdB (PDB entry 1X75), characterized by classic hydrogen bonds between the β strands in the interface (blue dashed lines). The orange conformation is observed in the $CcdB_2$:$CcdA^{37-72}$ complex in which the dimer interface opens up and a string of water molecules (red spheres) enters the interface, creating an alternative hydrogen bond network (orange dashed lines). Selected CcdB residues are labeled.

segments (Arg40-Gly63 and Ser64-Trp72). This allows segment Ser64-Trp72 to liberate the partially blocked binding epitope on CcdB, followed by a zippering of the Arg40-Gly63 segment into the binding groove. This would be impossible to accomplish by a more rigid prefolded protein domain.

A third fundamental property of intrinsically disordered proteins is that they can modulate their structures to fit multiple binding partners. This is exactly what happens during the consecutive binding of two $CcdA^{37-72}$ domains to the $CcdB_2$ dimer. It is not possible for $CcdA^{37-72}$ to engage in the second, low-affinity interaction with $CcdB_2$ using the same conformation that it adopts for the high-affinity interaction. Thus, again, this aspect of the mode of action of CcdA depends upon its intrinsically disordered nature.

Although the aforementioned observations are consistent with the established properties of intrinsically disordered proteins, there are also a number of unexpected aspects to the CcdA C terminus. Its unusually high affinity for CcdB, for example, sets CcdA apart from other intrinsically disordered proteins. These proteins are believed to be able to combine high specificity with low affinity, a feature that is of great importance in signaling functions. Here, the very high affinity of the first binding site ensures neutralization of the toxin even at very low concentrations of the antitoxin. CcdA also actively drives rejuvenation and changes the quaternary structure of its binding partner, contrasting with the notion of intrinsically disordered proteins being passive and moldable (Wright and Dyson, 1999). To our knowledge, this is the first intrinsically disordered protein that, upon binding, not only obtains a folded structure, but in addition significantly modulates the conformation of its binding partner.

Allostery Is a Fundamental Property of the Rejuvenation Process

Our experimental data indicate that rejuvenation is an allosteric process. Indeed, if rejuvenation has to work without an allosteric component, by increasing the apparent $CcdA_2$ concentration around the $CcdB_2$:$gyrase_2$ complex, ternary $gyrase_2$:$CcdB_2$:$CcdA_2$ intermediates with a measurable lifetime should be formed, involving interactions through segment Ser64-Trp72, but not through segment Arg40-Gly63. Despite intensive efforts to detect such a ternary complex by means of SPR, none was ever observed.

The kinetics of the rejuvenation process also indicate that CcdA acts as a key that unlocks gyrase rather than passively waiting until CcdB is released from gyrase. The half-life of the CcdB:gyrase complex is reduced to a few seconds after exposure to CcdA, while it is at least 5 hr in the absence of CcdA (Dao-Thi et al., 2005; Kampranis et al., 1999). It is expected that the off-rate for CcdB from gyrase is even smaller in the in vivo situation where CcdB is trapped in a complex involving not only the complete gyrase molecule consisting of two A and two B chains, but also covalently bound DNA and possibly the T-segment DNA strand trapped in an intermediate state. Thus, the lifetime of such a complex will be much too long compared to the in vivo half-life of 30 min of CcdA (Van Melderen et al., 1994). If the rejuvenation would involve competition for the same binding site without an allosteric component, the action of CcdA would be too slow to protect the cell against any accidentally activated CcdB and the rejuvenation activity would serve no purpose.

Rejuvenation and Transcription Regulation Are Mechanistically Linked

A long standing discussion concerns the physiological role of TA modules and, in particular, whether they are bacteriostatic or bacteriocidal. The complicated interactions in the *ccd* module,

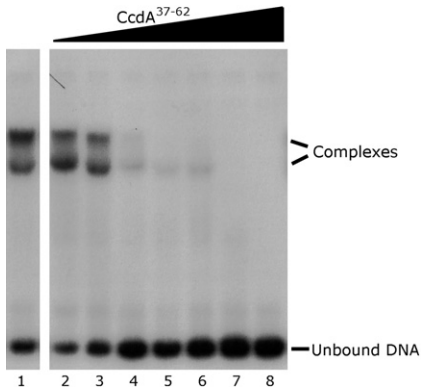

Figure 7. Binding of the CcdA:CcdB Complex to the O/P Region in the Presence of Competing Amounts of CcdA$^{37-62}$

Lane 1 (0.05 μM CcdA and 0.025 μM CcdB) serves as a positive control. Under the experimental conditions, a 1:1 CcdA:CcdB complex is formed that can shift the DNA (Afif et al., 2001). The two mobility-shifted complexes were also observed by Afif et al., 2001 and reflect the multiple binding sites on the O/P region. Lanes 2–8 all contain 0.05 μM CcdA and 0.025 μM CcdB incubated with increasing amounts of CcdA$^{37-62}$ (0.1, 0.15, 0.20, 0.8, 3.2, 12.8, and 100 μM, respectively). Addition of an excess of this fragment disrupts the shift of the DNA fragment. These concentrations are significantly lower than the ~15 mM that is theoretically required to disrupt 50% of the high-affinity interactions (involving residues 40–72 of CcdA) in the CcdA:CcdB complex.

which integrate rejuvenation and transcription regulation, is more consistent with a reversible regulation mechanism than with a one-way trigger for cell death. Figure 5 summarizes this regulatory network. While the high-affinity binding site is fundamental for the rejuvenation action of CcdA, the second, low-affinity binding site is at the heart of the autoregulation circuit. In the repressing operator complex, CcdB and CcdA are present in a 1:1 ratio and are believed to form a chain of alternating $CcdA_2$ and $CcdB_2$ dimers (Dao-Thi et al., 2002). For such a chain to form, both the high- and low-affinity binding sites of $CcdB_2$ need to be occupied (Figure 5). At high concentrations of CcdA, the second site will be occupied and repression of the *ccd* operon will start, preventing excessive production of CcdA and CcdB. When the cellular CcdA/CcdB ratio diminishes due to the proteolytic action of Lon on CcdA (Kampranis et al., 1999), excess CcdB will resolve the operator complex to form a soluble hexameric nonrepressing $CcdB_2$:$CcdA_2$:$CcdB_2$ complex (Afif et al., 2001). In this process, high-affinity $CcdB_2$:$CcdA_2$ interactions replace the low-affinity interactions present in the operator complex, thus warranting the neutralization of CcdB during derepression. Following transcription, higher levels of CcdA than CcdB are produced due to translational coupling (Miki et al., 1984). As the CcdA pool gets replenished, the empty low-affinity binding sites on $CcdB_2$ are resaturated and the repressive mode is restored.

The *ccd* module thus uses a unusual mechanism of gene regulation in which the same protein (CcdB) can act both as a corepressor or a coactivator. This is distinct from the classical mechanisms involving a repressor or activator controlled by sensing a small molecule ligand or from other complex regulatory systems, such as the functioning of the lambda repressor (Lewin, 2000). It allows the *ccd* system to absorb fluctuations of the cellular levels of CcdA and CcdB and to tightly control their ratio, preventing accidental activation of CcdB.

Table 1. Crystallographic Data Collection and Refinement Statistics

	$CcdB_2$:$CcdA^{37-72}$	$CcdB_2$:$CcdA^{37-72}{}_2$
Data Collection		
Space group	$P2_1$	$P2_1$
Cell dimensions		
a, b, c (Å)	41.4, 38.0, 69.7	58.2, 38.4, 62.5
α, β, γ (°)	90.0, 97.5, 90.0	90.0, 94.7, 90.0
Resolution (Å)	15.78-1.45 (1.50-1.45)	32.6-2.35 (2.43-2.35)
R_{sym} (%)	0.043 (0.107)	0.142 (0.297)
I/σ(I)	18.35 (7.95)	7.7 (2.9)
Completeness (%)	95.9 (98.2)	80.9 (64.6)[a]
Redundancy	2.9 (2.9)	3.5 (3.1)
Wavelength (Å)	0.8423	0.9801
Refinement		
No. reflections	34773	9424
R_{work}/R_{free}	0.165/0.203	0.203/0.272
No. atoms		
Protein	1918	2092
Water	329	113
Rms deviations		
Bond angles (°)	1.20	1.04
Bond length (Å)	0.009	0.011

Values between parentheses correspond to the highest resolution shell.
[a] The low completeness is in part due to the geometry of the detector. In the resolution range 5.0–3.2 Å, the completeness is over 90%.

EXPERIMENTAL PROCEDURES

Proteins and Peptides

Concentrations of CcdB and gyrase fragments are given as dimer equivalents. The concentration of the CcdA-derived peptides is in monomer equivalents. All peptides were obtained from Bio-Synthesis (Lewisville, TX, USA) and are over 90% pure. CcdB, GyrA14, and GyrA59 were purified as described (Buts et al., 2005a; Dao-Thi et al., 2004; Reece and Maxwell, 1991).

Crystallography

Crystals for both complexes were obtained when equal volumes of complex (for the $CcdB_2$:$CcdA^{37-72}$, a ratio of 1:1 was used and for the $CcdB_2$:$CcdA^{37-72}{}_2$ complex, a ratio of 1:5 was used) and precipitant solution containing 22% PEG4000, 100 mM Tris (pH 7.4), and 200 mM $LiSO_4$ were mixed at 20°C and equilibrated against 0.5 ml of the precipitant solution. After soaking in 100 mM Tris (pH 7.4), 200 mM $LiSO_4$, and 35% PEG4000, a crystal was flash-frozen at 100°K in a nitrogen stream. Data were collected at EMBL beamline BW7B at the DESY, Hamburg, and at the PROXIMA1 beamline at the SOLEIL synchrotron, Gif-Sur-Yvette. Data were processed using the HKL package (Otwinowski, 1997). A first model was built automatically with ARP/wARP (Perrakis et al., 2001), with $CcdB_2$ as a search model (1VUB). Refinement was performed with REFMAC 5.0 (Murshudov et al., 1997) from the CCP4 program suite (Collaborative Computational Project, 1994). Data collection and refinement statistics are given in Table 1.

SPR Experiments

SPR experiments were performed on a Biacore3000 system (GE Healthcare) at 25°C in HBS buffer and a flow rate of 30 μl/minute.

For kinetic experiments, CcdB was immobilized on a CM5 sensor chip via amine coupling in 10 mM sodium acetate buffer (pH 5.0). $CcdA^{37-72}$ was injected in concentrations between 4.9 nM and 76.5 pM, $CcdA^{37-62}$ in concentrations between 53.6 μM and 1.7 μM,and $CcdA^{65-72}$ in concentrations between 32.5 μM and 0.25 μM. Association was observed for 180 s and dissociation for at least 150 s. Regeneration was done with 10 μl 10 mM glycine (pH 1.5). The binding data were analyzed with the BIAevaluation 4.1 software.

For rejuvenation experiments, GyrA59 and GyrA14 were immobilized on a CM5 sensor chip via amine coupling in 10 mM sodium acetate (pH 4.9). 35 μl of 1 mM CcdB was injected followed by 60 μl $CcdA^{37-72}$ (6 nM) or $CcdA^{65-72}$ (650 μM) (these concentrations equal 20 times the K_D).

CD Spectroscopy of $CcdA^{37-72}$

CD spectra were recorded on a J-715 spectropolarimeter (Jasco). Scans were taken using a 1 mm cuvette, a scan rate of 50 nm/min, a band width of 1.0 nm, and a resolution of 1.0 nm. One hundred accumulations were taken at 25°C. For the far UV spectra (185–270 nm), a concentration of 9.1 μM $CcdB_2$:$CcdA^{37-72}$, $CcdA^{37-72}$, and CcdB in 50 mM phosphate (pH 7.5) and 100 mM NaF was used. For the near UV spectra (250–310 nm) a concentration of 114.4 μM of $CcdA^{37-72}$ in water was used.

CD and Fluorescence Titrations of $CcdA^{37-72}$, $CcdA^{37-62}$, and $CcdA^{65-72}$ to $CcdB_2$

Far UV CD spectra were taken with the same parameters described above except for the resolution that was set to 0.2 nm. Fluorescence measurements were done on a PerkinElmer LS 55 Luminescence spectrometer in a 10 mm cuvette. For each point, six spectra were accumulated between 300 and 400 nm upon excitation at 295 nm. CD and fluorescence titrations were done at 25°C using 5.5 μM (for CD) and 4 μM (for fluorescence) $CcdB_2$ in 50 mM phosphate (pH 7.5) and 100 mM NaF. Stock solutions of $CcdA^{37-72}$, $CcdA^{37-62}$, and $CcdA^{65-72}$ used for titrations were 0.17, 0.27, and 1.9 mM in the same buffer.

The molar residue ellipticity at 210 nm for the CD titrations and the emission at 356 nm for the fluorescence titrations were plotted against the peptide concentration. These plots were corrected for buffer and free peptide and fitted with the equations described in the next section.

Analysis of the Binding of $CcdA^{37-72}$ to $CcdB_2$

The sequential binding of $CcdA^{37-72}$ to $CcdB_2$ is described with Adair's equations (Adair, 1925; Koshland et al., 1966). With

$$CcdB_2 + CcdA^{37-72} \overset{K_1}{\longleftrightarrow} CcdB_2 : CcdA^{37-72}$$

$$CcdB_2 : CcdA^{37-72} + CcdA^{37-72} \overset{K_2}{\longleftrightarrow} CcdA^{37-72} : CcdB_2 : CcdA^{37-72}$$

$$K_1 = \frac{\left[CcdB_2\right]\left[CcdA^{37-72}\right]}{\left[CcdB_2 : CcdA^{37-72}\right]} \quad (1)$$

$$K_2 = \frac{\left[CcdB_2 : CcdA^{37-72}\right]\left[CcdA^{37-72}\right]}{\left[CcdA^{37-72} : CcdB_2 : CcdA^{37-72}\right]} \quad (2)$$

The fraction of $CcdA^{37-72}$ bound to CcdB (α) can be expressed as:

$$\alpha = \frac{K_1^{-1}\left[CcdA^{37-72}\right] + 2K_1^{-1}K_2^{-1}\left[CcdA^{37-72}\right]^2}{\left(1 + K_1^{-1}\left[CcdA^{37-72}\right] + K_1^{-1}K_2^{-1}\left[CcdA^{37-72}\right]^2\right)} \quad (3)$$

This equation can then be fitted to the experimental binding curve obtained by monitoring the changes in molar ellipticity upon binding $CcdA^{37-72}$ to $CcdB_2$, using Levenberg-Marquardt minimization (Press et al., 1992).

Considering that $K_1 \ll K_2$, Equation 3 can be further simplified depending on the concentration $CcdA^{37-72}$ used in the measurement:

For the SPR measurement $[CcdA^{37-72}] \ll K_2$

$$\alpha = \frac{K_1K_2}{K_1K_2}\frac{\left(\left(K_2 + 2\left[CcdA^{37-72}\right]\right)\left[CcdA^{37-72}\right]\right)}{\left(K_1K_2 + \left[CcdA^{37-72}\right]\left(K_2 + \left[CcdA^{37-72}\right]\right)\right)} = \frac{\left(K_2 + 2\left[CcdA^{37-72}\right]\right)\left[CcdA^{37-72}\right]}{\left(K_1K_2 + \left[CcdA^{37-72}\right]\left(K_2 + \left[CcdA^{37-72}\right]\right)\right)}$$

We then assume that $(K_2+[CcdA^{37-72}]) = K_2$:

$$\alpha = \frac{\left(K_2\left[CcdA^{37-72}\right]\right)}{\left(K_1K_2 + \left[CcdA^{37-72}\right]K_2\right)} = \frac{\left[CcdA^{37-72}\right]}{K_1 + \left[CcdA^{37-72}\right]} \quad (4)$$

For the CD measurements $[CcdA^{37-72}] \gg K_1$

$$\alpha = \frac{K_1K_2}{K_1K_2}\frac{\left(\left(K_2 + 2\left[CcdA^{37-72}\right]\right)\left[CcdA^{37-72}\right]\right)}{\left(K_1K_2 + \left[CcdA^{37-72}\right]\left(K_2 + \left[CcdA^{37-72}\right]\right)\right)} = \frac{K_2\left[CcdA^{37-72}\right] + 2\left[CcdA^{37-72}\right]^2}{K_2\left(K_1 + \left[CcdA^{37-72}\right]\right) + \left[CcdA^{37-72}\right]^2}$$

We then assume that $(K_1+[CcdA^{37-72}]) = [CcdA^{37-72}]$:

$$\alpha = \frac{\left(K_2\left[CcdA^{37-72}\right] + 2\left[CcdA^{37-72}\right]^2\right)}{\left(K_2\left[CcdA^{37-72}\right] + \left[CcdA^{37-72}\right]^2\right)} = 1 + \frac{\left(\left[CcdA^{37-72}\right]\right)}{\left(K_2 + \left[CcdA^{37-72}\right]\right)} \quad (5)$$

NMR Spectroscopy

NMR spectra were acquired on 1 mg $CcdA^{37-72}$ in 50 mM phosphate (pH 6.5), 80 mM NaCl, 0.02% NaN_3 in 90% H_2O/10% D_2O at 25°C on a Varian Unity INOVA 600 MHz NMR spectrometer. Thirty-two scans were accumulated for each of the 256 increments of the TOCSY and NOESY spectra and referenced relative to external DSS. The TOCSY spectrum was acquired with a mixing time of 40 ms, while 150 ms was used for the NOESY. All spectra were processed with nmrPipe and analyzed with NMRVIEW. Two-dimensional TOCSY and NOESY spectra were used to assign the unlabeled $CcdA^{37-72}$. For each residue, the residue-specific average of the absolute differences between the measured and the corresponding random coil values ($\Sigma|\delta_{exp}-\delta_{random}|$) was calculated.

Analytical Gel Filtration

The analytical gel filtrations were done on a Superdex 200HR 10/30 column at a flow rate of 0.5 ml/min. The running buffer was 20 mM Tris (pH 7.0), 150 mM NaCl, 1 mM EDTA. The $GyrA59_2$:$CcdB_2$ complex was formed and purified on a Superdex 200HR 10/30 column and concentrated to 80 μM. To prepare the sample, 200 μl buffer or one equivalent of $CcdA^{37-72}$ was added to 60 μl $GyrA59_2$:$CcdB_2$ complex. All samples were run immediately and the identity of the peaks was confirmed by running a Coomassie-stained SDS-PAGE with the Mark12 Unstained Standard (Invitrogen) as a marker.

In Vivo Antitoxin Activity Assays

E. coli BW27783 cells, cotransformed with plasmids containing the CcdB toxin (chloramphenicol resistant) and the test construct (ampicillin resistant) (for details on the cloning of these vectors see Table S1), were grown overnight in LB medium with 100 μg/ml ampicillin, 25 μg/ml chloramphenicol, and 0.2% glucose. Dilutions (up to 10^{-7}) were prepared in 200 mM $MgCl_2$, and 20 μl of each dilution was spotted on to agar plates containing 100 μg/ml ampicillin, 25 μg/ml chloramphenicol, and either 0.2% glucose (to repress expression of both the toxin and the antitoxin genes) or 0.2% L-arabinose (to induce expression of both the toxin and the antitoxin genes). Overnight grown colonies were counted, and the efficiency of plating was calculated as the ratio of CFU per milliliter in the presence of inducer and CFU per milliliter in the presence of repressor. The results are the means of three independent experiments.

ITC Experiments

ITC titrations were carried out on a Microcal Omega ITC. Prior to the measurement, the CcdB was dialyzed to 50 mM phosphate (pH 7.5) and 150 mM NaCl. $CcdA^{37-72}$ was first dissolved in a small amount of water and diluted to the same phosphate buffer. The titrations were carried out at 25°C, injecting 142.6 μM CcdB into 11.3 μM $CcdA^{37-72}$ (reverse direction) or 8 μM CcdB into 187.2 μM $CcdA^{37-72}$ (forward direction). The forward and reverse titrations were fitted using a shared two-step binding model, with each step characterized by the association constant $K_{A,1/2}$ and the standard enthalpy change $\Delta H_{1/2}$. The equilibrium constants and mass balances were expressed as a system of simultaneous constraints and solved using standard linear algebra techniques to provide the system composition in function of the progress of the simulated titration.

EMSA Experiments

The (5′-^{32}P) single-end-labeled DNA fragment used for the EMSA is a 130 bp DNA fragment containing the 113 bp operator-promotor region of the *ccd* operon. The ccdOP1 primer (5′- GTCAACTGTCACTGTAATACGCT GCTTC AT-3′) was labeled with [γ ^{32}P]-ATP (Perkin Elmer) and T4 polynucleotide kinase (Fermentas). The single-end-labeled DNA fragment was obtained by PCR using the pDONR221 vector as template with the labeled ccdOP1 and the ccdOP2 primer (5′- CATAAGGCTTACTAAAAGCCAGATAACAGT-3′) and with the ready-to-go Taq DNA polymerase system (Sigma). The 5′ single-end-labeled DNA fragments were purified by 6% polyacrylamide gel electrophoresis.

CcdA, $CcdA^{37-62}$,CcdB, labeled DNA (15,000 cpm), and 0.1 μg sonicated herring sperm DNA were mixed respectively in 30 mM Tris (pH 7.5), 200 mM NaCl, 15 mM $MgCl_2$, and 150 μg/ml BSA. Binding reactions were carried out in 15 μl at 20°C for 20 min. After incubation, 3 μl loading buffer (25% ficoll, 0.1% xylenexyanol, and 0.1% bromophenol) was added to each sample. EMSA were performed on 6% polyacrylamide gels prepared with TBE running buffer. Electrophoresis was performed at 7 V/cm for 3 hr.

ACCESSION NUMBERS

Atomic coordinates and structure factors for the reported crystal structure have been deposited with the Protein Data Bank under accession code 3HPW and 3G7Z.

SUPPLEMENTAL DATA

Supplemental Data include Supplemental Experimental Procedures, six figures, and one table and can be found with this article online at http://www.cell.com/molecular-cell/supplemental/S1097-2765(09)00386-4.

ACKNOWLEDGMENTS

This work was supported by VIB, the Onderzoeksraad of the VUB, and by research grants from FWO-Vlaanderen. N.D.J. received financial support from IWT. L.B. is a postdoctoral fellow of the FWO-Vlaanderen. K.Z. thanks the Austrian Science Foundation (FWF) for financial support under project number 19902. The authors acknowledge the use of EMBL beamline BW7B (DESY, Hamburg, Germany) and the beamline Proxima1 (SOLEIL, Paris, France). The authors wish to thank Julie Bouckaert for help with the SPR measurements and Jan Steyaert for critically reading the manuscript.

Received: November 6, 2008
Revised: April 14, 2009
Accepted: May 21, 2009
Published: July 30, 2009

REFERENCES

Adair, G.S. (1925). The hemoglobin system. VI. The oxygen dissociation curve of hemoglobin. J. Biol. Chem. *63*, 529–545.

Afif, H., Allali, N., Couturier, M., and Van Melderen, L. (2001). The ratio between CcdA and CcdB modulates the transcriptional repression of the *ccd* poison-antidote system. Mol. Microbiol. *41*, 73–82.

Alonso, J.C., Balsa, D., Cherny, I., Christensen, S.K., Espinosa, M., Francuski, D., Gazit, E., Gerdes, K., Hitchin, E., Martin, T.M., et al. (2007). Bacterial Toxin-Antitoxin systems as targets for the development of novel antibiotics. In Enzyme-mediated resistance to antibiotics M. Tolmasky and R.A. Bonomo, eds. (West Sussex, England: Blackwell Science), pp. 313–329.

Bernard, P., and Couturier, M. (1991). The 41 carboxy-terminal residues of the miniF plasmid CcdA protein are sufficient to antagonize the killer activity of the CcdB protein. Mol. Gen. Genet. *226*, 297–304.

Bernard, P., and Couturier, M. (1992). Cell killing by the F plasmid CcdB protein involves poisoning of DNA-topoisomerase II complexes. J. Mol. Biol. *226*, 735–745.

Bernard, P., Kezdy, K.E., Van Melderen, L., Steyaert, J., Wyns, L., Pato, M.L., Higgins, P.N., and Couturier, M. (1993). The F-Plasmid CcdB Protein Induces Efficient ATP-Dependent DNA Cleavage by Gyrase. J. Mol. Biol. *234*, 534–541.

Buts, L., De Jonge, N., Loris, R., Wyns, L., and Dao-Thi, M.H. (2005a). Crystallization of the C-terminal domain of the addiction antidote CcdA in complex with its toxin CcdB. Acta Crystallogr. Sect. F Struct. Biol. Cryst. Commun. *61*, 949–952.

Buts, L., Lah, J., Dao-Thi, M.H., Wyns, L., and Loris, R. (2005b). Toxin-antitoxin modules as bacterial metabolic stress managers. Trends Biochem. Sci. *30*, 672–679.

Collaborative Computational Project, N.4. (1994). The CCP4 suite: programs for protein crystallography. Acta Crystallogr. D Biol. Crystallogr. *50*, 760–763.

Critchlow, S.E., O'Dea, M.H., Howells, A.J., Couturier, M., Gellert, M., and Maxwell, A. (1997). The interaction of the F plasmid killer protein, CcdB, with DNA gyrase: induction of DNA cleavage and blocking of transcription. J. Mol. Biol. *273*, 826–839.

Dao-Thi, M.H., Charlier, D., Loris, R., Maes, D., Messens, J., Wyns, L., and Backmann, J. (2002). Intricate interactions within the ccd plasmid addiction system. J. Biol. Chem. *277*, 3733–3742.

Dao-Thi, M.H., Van Melderen, L., De Genst, E., Buts, L., Ranquin, A., Wyns, L., and Loris, R. (2004). Crystallization of CcdB in complex with a GyrA fragment. Acta Crystallogr. D Biol. Crystallogr. *60*, 1132–1134.

Dao-Thi, M.H., Van Melderen, L., De Genst, E., Afif, H., Buts, L., Wyns, L., and Loris, R. (2005). Molecular basis of gyrase poisoning by the addiction toxin CcdB. J. Mol. Biol. *348*, 1091–1102.

Dong, K.C., and Berger, J.M. (2007). Structural basis for gate-DNA recognition and bending by type IIA topoisomerases. Nature *450*, 1201–1205.

Dunker, A.K., and Uversky, V.N. (2008). Signal transduction via unstructured protein conduits. Nat. Chem. Biol. *4*, 229–230.

Engelberg-Kulka, H., and Glaser, G. (1999). Addiction modules and programmed cell death and antideath in bacterial cultures. Annu. Rev. Microbiol. *53*, 43–70.

Engelberg-Kulka, H., Sat, B., Reches, M., Amitai, S., and Hazan, R. (2004). Bacterial programmed cell death systems as targets for antibiotics. Trends Microbiol. *12*, 66–71.

Fass, D., Bogden, C.E., and Berger, J.M. (1999). Quaternary changes in topoisomerase II may direct orthogonal movement of two DNA strands. Nat. Struct. Biol. *6*, 322–326.

Gerdes, K. (2000). Toxin-antitoxin modules may regulate synthesis of macromolecules during nutritional stress. J. Bacteriol. *182*, 561–572.

Gerdes, K., Christensen, S.K., and Lobner-Olesen, A. (2005). Prokaryotic toxin-antitoxin stress response loci. Nat. Rev. Microbiol. *3*, 371–382.

Johnson, E.P., Strom, A.R., and Helinski, D.R. (1996). Plasmid RK2 toxin protein ParE: purification and interaction with the ParD antitoxin protein. J. Bacteriol. *178*, 1420–1429.

Kampranis, S.C., Howells, A.J., and Maxwell, A. (1999). The interaction of DNA gyrase with the bacterial toxin CcdB: evidence for the existence of two gyrase-CcdB complexes. J. Mol. Biol. *293*, 733–744.

Kolodkin-Gal, I., Hazan, R., Gaathon, A., Carmeli, S., and Engelberg-Kulka, H. (2007). A linear pentapeptide is a quorum-sensing factor required for *mazEF*-mediated cell death in *Escherichia coli*. Science *318*, 652–655.

Koshland, D.E., Jr., Nemethy, G., and Filmer, D. (1966). Comparison of experimental binding data and theoretical models in proteins containing subunits. Biochemistry *5*, 365–385.

Lewin, B. (2000). Genes VII (New York: Oxford Univ. Press and Cell Press).

Loris, R., Dao-Thi, M.H., Bahassi, E.M., Van Melderen, L., Poortmans, F., Liddington, R., Couturier, M., and Wyns, L. (1999). Crystal structure of CcdB, a topoisomerase poison from *E. coli*. J. Mol. Biol. *285*, 1667–1677.

Madl, T., Van Melderen, L., Mine, N., Respondek, M., Oberer, M., Keller, W., Khatai, L., and Zangger, K. (2006). Structural basis for nucleic acid and toxin recognition of the bacterial antitoxin CcdA. J. Mol. Biol. *364*, 170–185.

Magnuson, R., and Yarmolinsky, M.B. (1998). Corepression of the P1 addiction operon by Phd and Doc. J. Bacteriol. *180*, 6342–6351.

Magnuson, R.D. (2007). Hypothetical functions of toxin-antitoxin systems. J. Bacteriol. *189*, 6089–6092.

Maki, S., Takiguchi, S., Horiuchi, T., Sekimizu, K., and Miki, T. (1996). Partner switching mechanisms in inactivation and rejuvenation of *Escherichia coli* DNA gyrase by F plasmid proteins LetD (CcdB) and LetA (CcdA). J. Mol. Biol. *256*, 473–482.

Miki, T., Yoshioka, K., and Horiuchi, T. (1984). Control of cell division by sex factor F in *Escherichia coli*. I. The 42.84–43.6 F segment couples cell division of the host bacteria with replication of plasmid DNA. J. Mol. Biol. *174*, 605–625.

Monti, M.C., Hernandez-Arriaga, A.M., Kamphuis, M.B., Lopez-Villarejo, J., Heck, A.J., Boelens, R., Diaz-Orejas, R., and van den Heuvel, R.H. (2007). Interactions of Kid-Kis toxin-antitoxin complexes with the *parD* operator-promoter region of plasmid R1 are piloted by the Kis antitoxin and tuned by the stoichiometry of Kid-Kis oligomers. Nucleic Acids Res. *35*, 1737–1749.

Morais Cabral, J.H., Jackson, A.P., Smith, C.V., Shikotra, N., Maxwell, A., and Liddington, R.C. (1997). Crystal structure of the breakage-reunion domain of DNA gyrase. Nature *388*, 903–906.

Murshudov, G.N., Vagin, A.A., and Dodson, E.J. (1997). Refinement of macromolecular structures by the maximum-likelihood method. Acta Crystallogr. D Biol. Crystallogr. *53*, 240–255.

Nariya, H., and Inouye, M. (2008). MazF, an mRNA interferase, mediates programmed cell death during multicellular *Myxococcus* development. Cell *132*, 55–66.

Otwinowski, Z.M.W. (1997). Processing of X-ray diffraction data collected in oscillation mode. Methods Enzymol. *257*, 307–326.

Overgaard, M., Borch, J., Jorgensen, M.G., and Gerdes, K. (2008). Messenger RNA interferase RelE controls relBE transcription by conditional cooperativity. Mol. Microbiol. *69*, 841–857.

Pandey, D.P., and Gerdes, K. (2005). Toxin-antitoxin loci are highly abundant in free-living but lost from host-associated prokaryotes. Nucleic Acids Res. *33*, 966–976.

Perrakis, A., Harkiolaki, M., Wilson, K.S., and Lamzin, V.S. (2001). ARP/wARP and molecular replacement. Acta Crystallogr. D Biol. Crystallogr. *57*, 1445–1450.

Press, W.H., Teukolsky, S.A., Vetterling, W.T., and Flannery, B.P. (1992). Numerical Recipes in C. The Art of Scientific Computing. (New York: Cambridge University Press).

Reece, R.J., and Maxwell, A. (1991). Probing the limits of the DNA breakage-reunion domain of the *Escherichia coli* DNA gyrase A protein. J. Biol. Chem. *266*, 3540–3546.

Tam, J.E., and Kline, B.C. (1989a). Control of the *ccd* operon in plasmid F. J. Bacteriol. *171*, 2353–2360.

Tam, J.E., and Kline, B.C. (1989b). The F plasmid ccd autorepressor is a complex of CcdA and CcdB proteins. Mol. Gen. Genet. *219*, 26–32.

Van Melderen, L., Bernard, P., and Couturier, M. (1994). Lon-dependent proteolysis of CcdA is the key control for activation of CcdB in plasmid-free segregant bacteria. Mol. Microbiol. *11*, 1151–1157.

Williams, J.J., and Hergenrother, P.J. (2008). Exposing plasmids as the Achilles' heel of drug-resistant bacteria. Curr. Opin. Chem. Biol. *12*, 389–399.

Wright, P.E., and Dyson, H.J. (1999). Intrinsically unstructured proteins: reassessing the protein structure-function paradigm. J. Mol. Biol. *293*, 321–331.

Molecular Cell, Volume *35*

Supplemental Data

Rejuvenation of CcdB-Poisoned Gyrase by an Intrinsically Disordered Protein Domain

Natalie De Jonge, Abel Garcia-Pino, Lieven Buts, Sarah Haesaerts, Daniel Charlier, Klaus Zangger, Lode Wyns, Henri De Greve, and Remy Loris

SUPPLEMENTAL EXPERIMENTAL PROCEDURES

$CcdA^{37-72}$ folds upon binding to $CcdB_2$

In solution, $CcdA^{37-72}$, the isolated C-terminal domain of CcdA, behaves as a monomeric and intrinsically disordered protein. Far and near UV CD spectra are characteristic of random coil conformations and no unfolding transition can be observed with DSC (thermal unfolding, data not shown) or fluorescence (chemical unfolding) measurements (Figure S1). Two-dimensional TOCSY and NOESY spectra show that the proton frequencies of all backbone amide protons of $CcdA^{37-72}$ are characterized by poor chemical shift dispersion. Only trivial intraresidue and sequential NOEs could be observed, further corroborating absence of tertiary structure in free $CcdA^{37-72}$. The residue-specific average of the absolute differences between the measured shifts and the corresponding random coil values clearly show that $CcdA^{37-72}$ has no tendency towards α-helical conformations in accordance with previous measurements on the intact $CcdA_2$ dimer (Figure S2) (Madl *et al.*, 2006).

Upon addition of $CcdA^{37-72}$ to $CcdB_2$, the CD spectrum of $CcdA^{37-72}$ undergoes significant changes. Figure S1A compares the far UV CD spectrum of $CcdA^{37-72}$ in its free state and in complex with a CcdB dimer ($CcdB_2$:$CcdA^{37-72}$ ratio 1:1). The latter indicates that upon complex formation $CcdA^{37-72}$ folds to a largely α-helical conformation, in agreement with our crystallographic studies.

SUPPLEMENTAL DATA

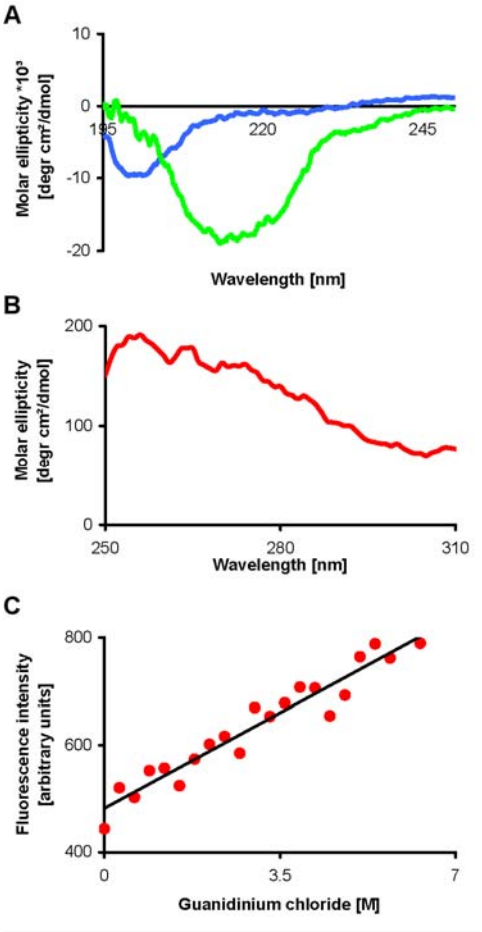

Figure S1. **CcdA$^{37\text{-}72}$ is intrinsically disordered**

(A) Far UV CD spectra of CcdA$^{37\text{-}72}$ at 25 °C. The spectrum in blue is of unbound CcdA$^{37\text{-}72}$ and has the typical shape of a random coil spectrum. The spectrum in green is the difference spectrum between the $CcdB_2$:CcdA$^{37\text{-}72}$ complex and $CcdB_2$, thus corresponding to that of CcdA$^{37\text{-}72}$ in its bound state. Here the typical spectral shape corresponding to α-helix is clearly visible.

(B) The near UV CD spectrum of CcdA$^{37\text{-}72}$ lacks sharp peaks, which is an indication of disorder.

(C) Fluorescence spectroscopy measurements of $CcdA^{37-72}$ show a monotonic increase upon chemical unfolding with guanidinium chloride and the absence of a discrete folding/unfolding transition.

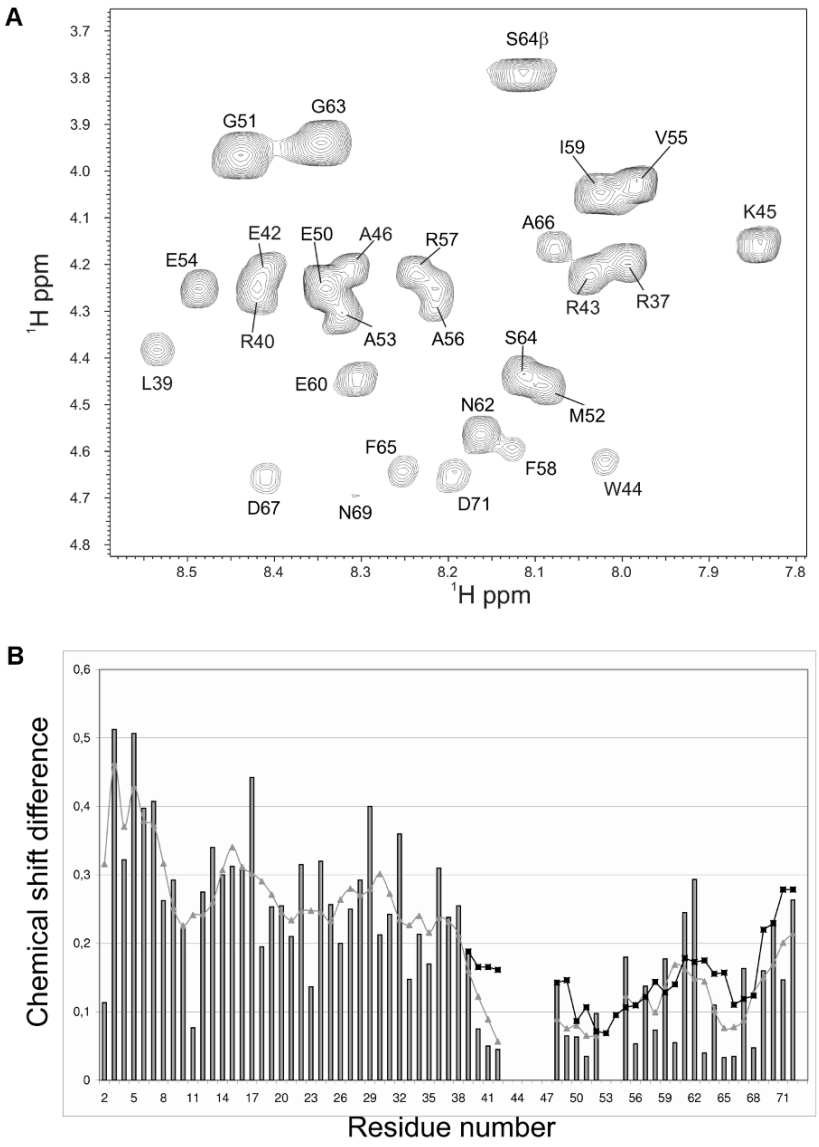

Figure S2. **Solution NMR studies on CcdA$^{37-72}$**

(A) The fingerprint region of the TOCSY spectrum of CcdA$^{37-72}$ shows poor chemical shift dispersion. They all fall in the range between 7.8-8.6 ppm, typical for random coil conformations. Missing signals (e.g. E68 and R70) are likely the result of exchange broadening.

(B) Histogram of deviations from random coil values of proton chemical shifts versus the sequence number of full length CcdA. The five residue floating average (from residue i-2 to i+2), showing the trend is drawn by connected grey triangles. The values of CcdA$^{37-72}$ (dark

black squares) parallel the absolute chemical shift differences found in the C-terminal domain of full-length CcdA (Madl *et al.*, 2006), which is also unstructured in the absence of CcdB.

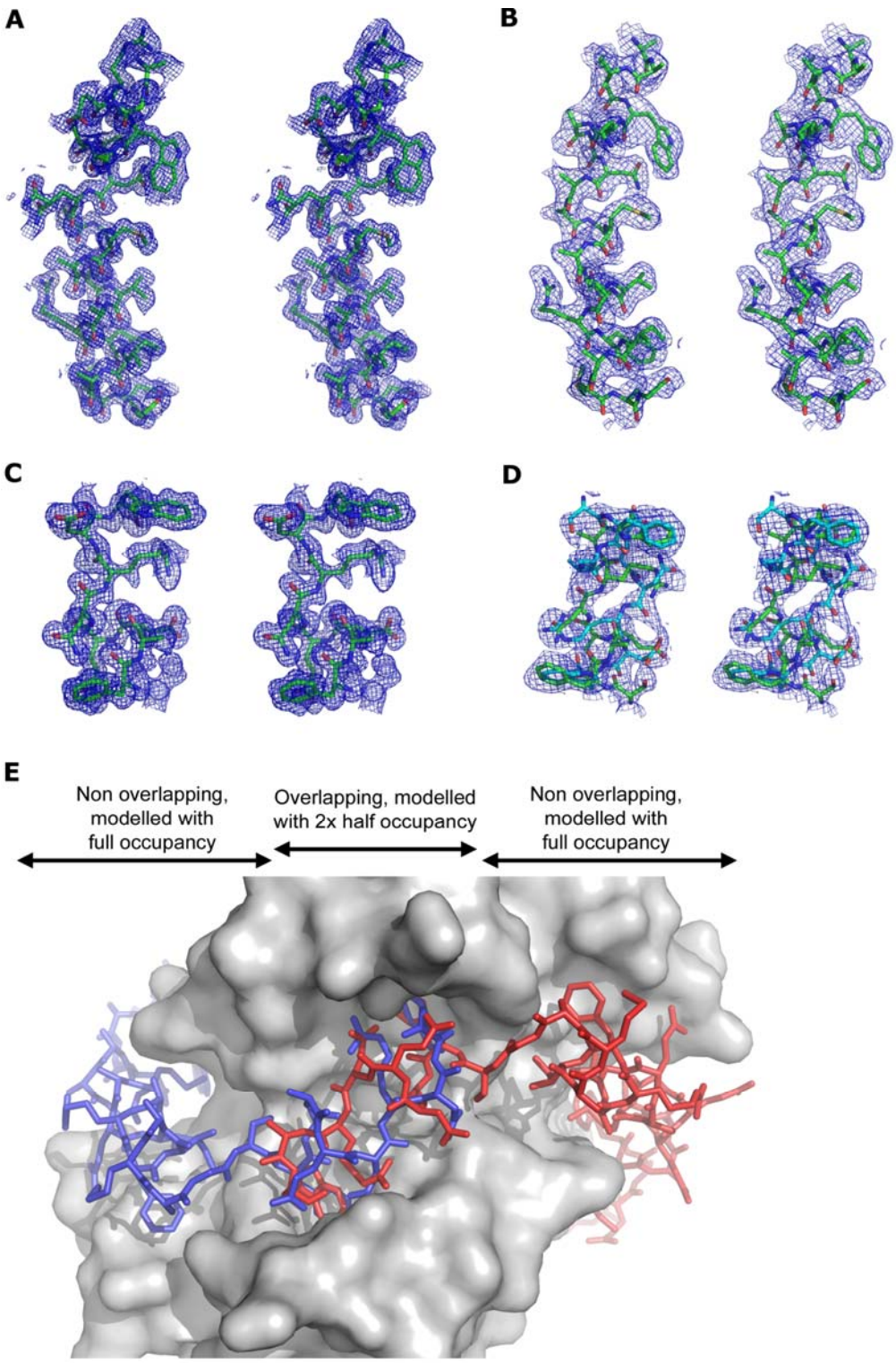

Figure S3. Electron density maps of the CcdA$^{37-72}$ segments from the CcdB$_2$:CcdA$^{37-72}$ and the CcdB$_2$:CcdA$^{37-72}{}_2$ complexes

The $2F_o$-F_c omit electron density maps (0.5 σ) of **(A)** the Arg40-Gly63 segment of the $CcdA^{37\text{-}72}$ domain in the $CcdB_2$:$CcdA^{37\text{-}72}{}_2$ structure, **(B)** the Ser64-Trp72 segment of the $CcdA^{37\text{-}72}$ domain in the $CcdB_2$:$CcdA^{37\text{-}72}{}_2$ structure, **(C)** the Arg40-Gly63 segment of the $CcdA^{37\text{-}72}$ domain in the $CcdB_2$:$CcdA^{37\text{-}72}{}_2$ structure, **(D)** the Ser64-Trp72 segment of both $CcdA^{37\text{-}72}$ domains in the $CcdB_2$:$CcdA^{37\text{-}72}{}_2$ structure. One segment is shown in green, while the other segment is shown in cyan. **(E)** Overlap between the two $CcdA^{37\text{-}72}$ binding sites. The surface of the $CcdB_2$ dimer is shown in gray. One $CcdA^{37\text{-}72}$ fragment is shown in red stick representation; the other $CcdA^{37\text{-}72}$ is shown in blue stick representation. The regions that were modeled with full and half occupancy are indicated.

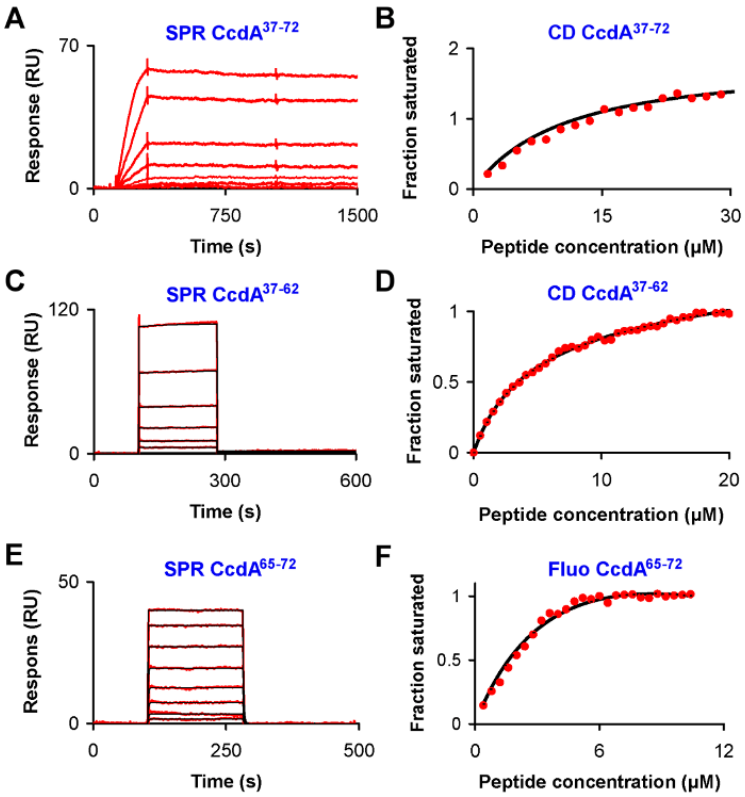

Figure S4. Affinity measurements of CcdA$^{37-72}$, CcdA$^{37-62}$ and CcdA$^{65-72}$ to CcdB$_2$

The data are shown in red, and the fittings are displayed in black.

(A) SPR measurements of CcdA$^{37-72}$ binding to CcdB$_2$ detect the high affinity binding site of 20 pM. CcdB$_2$ was immobilized on the chip and CcdA$^{37-72}$ was injected in concentrations between 4.9 nM and 76.5 pM. These concentrations do not allow for the detection of the low affinity binding site.

(B) CD titration where done keeping the concentration of CcdB$_2$ fixed at 5.5 µM and titrating in increasing amounts of CcdA$^{37-72}$. The binding curve shows the presence of two binding events. The first binding event corresponds to the high affinity binding event seen in SPR but its affinity constant cannot be obtained from the CD titration data. The second binding event corresponds to an affinity constant of 13 µM.

(C) SPR measurements of CcdA$^{37-62}$ binding to CcdB$_2$ give two roughly equal affinities of 3.0 µM and 29.0 µM.

(D) CD measurements of $CcdA^{37-62}$ binding on $CcdB_2$. A model for 2 binding sites on $CcdB_2$ was used to fit the experimental binding curves and results in two roughly similar affinities: 3.9 μM and 99.7 μM.

(E) SPR measurements of $CcdA^{65-72}$ binding on $CcdB_2$. A model for one binding site on $CcdB_2$ was used to fit the data and results in an affinity of 6.5 μM.

(F) Fluorescence measurements of $CcdA^{65-72}$ binding to $CcdB_2$ showing a single binding site with an affinity of 6.6 μM.

Figure S5. **Amino acid sequence of the A subunit of *E. coli* DNA gyrase**

The sequence encompassing the GyrA59 fragment is shown in orange and encompasses residues 1-523. The sequence of the GyrA14 fragment (which is part of GyrA59) encompasses residues 363-497. The surface representation of both fragments is shown in Figure 4B in the same colors.

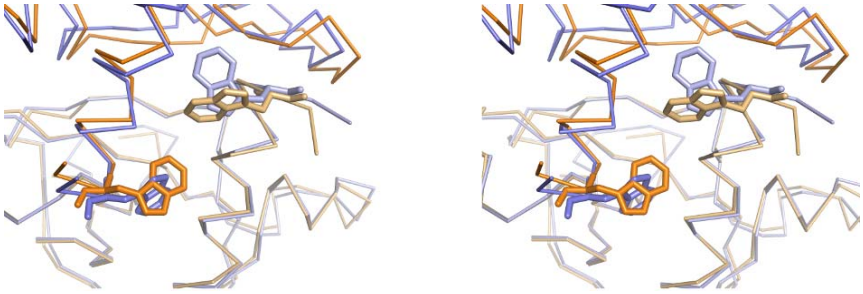

Figure S6. Movement of Trp99

Detail of the superposition of GyrA14-bound and $CcdA^{37-72}$-bound $CcdB_2$ with an emphasis on the movement of Trp99. The $CcdB_2$ dimer in its $CcdA^{37-72}$-bound conformation is shown in blue, while the GyrA14-bound conformation is shown in orange.

Table S1. *E. coli* strains and plasmids.

Bacterial strains or plasmids	Relevant characteristics and construction	Reference
<u>*E. coli* strains</u>		
CSH50gyrA462	CSH50 Δ(*lac-pro*), *ara*, *rps*, *thi*, *zeï-298*::Tn*10*, *gyrA462*	(Salmon *et al.*, 1994)
BW27783	*lacI*^{q} *rrnB3* Δ*lacZ4787 hsdR514* DE(*araBAD*)*567* DE(*rhaBAD*)*568* DE(*araFGH*) Φ(Δ*araEp* P_{CP8}-*araE*)	(Khlebnikov *et al.*, 2001)
<u>Plasmids</u>		
pBAD24	pBAD expression vector, Amp^R	(Guzman *et al.*, 1995)
pBADccdB-Cm^R	pBAD24 carrying CcdB. The gene was amplified by PCR with primers letB8 (CCCGAATTCAAAAGAGGTGTGCTATGCAG TTTAAGGTTTACACCTAT) and letB9 (CCCAAGCTTTTAT	This work

	ATTCCCCAGAACATCAGGTTA) and inserted in pBAD24 by using restriction enzymes HindIII and EcoRI. After cloning, the *bla* gene of the vector was replaced with the *cat* gene encoding chloramphenicol resistance	
pBADccdA	pBAD24 carrying CcdA. The gene was amplified by PCR with primers letA13 (CCCGAATTCAAAAGAGGTGTGCTATGA AGCAGCGTATTACAGTGACA) and letA26 (CCCAAGCTT TCACCAGTCCCTGTTCTCGTCAGCAAA) and inserted in pBAD24 by using restriction enzymes HindIII and EcoRI.	This work
pBADccdA$^{37\text{-}72}$	pBAD24 carrying CcdA$^{37\text{-}72}$. The gene was amplified by PCR with primers letA26 and letA37 (CCCGAATTCAAAAGAGGT GTGCTATGCGTCGTCTGCGTGCCGAACGCTGGAAAGCG) and inserted in pBAD24 by using restriction enzymes HindIII and EcoRI.	This work

Supplemental References

Guzman, L.M., Belin, D., Carson, M.J., and Beckwith, J. (1995). Tight regulation, modulation, and high-level expression by vectors containing the arabinose PBAD promoter. J. Bacteriol. *177*, 4121–4130.

Khlebnikov, A., Datsenko, K.A., Skaug, T., Wanner, B.L., and Keasling, J.D. (2001). Homogeneous expression of the P(BAD) promoter in Escherichia coli by constitutive expression of the low-affinity high-capacity AraE transporter. Microbiology *147*, 3241–3247.

Salmon, M.A., Van Melderen, L., Bernard, P., and Couturier, M. (1994). The antidote and autoregulatory functions of the F plasmid CcdA protein: a genetic and biochemical survey. Mol. Gen. Genet. *244*, 530–538.